Unsteady natural convection induced by constant surface cooling in a reservoir

Tomasz P. Bednarz[1] Chengwang Lei[2]
John C. Patterson[3]

(Received 8 August 2006; revised 7 January 2008)

Abstract

This article concerns numerical simulations of unsteady natural convection induced by constant cooling at the water surface of a reservoir. Numerical computations reveal the occurrence of sinking cold water plumes soon after the initiation of cooling. These sinking plumes are responsible for an initial mixing over the local water depth, resulting later in a distinct horizontal temperature gradient with the water temperature decreasing toward the shallow region due to the presence of a sloping boundary. Simulations also show that the relatively higher cooling rate in the shallow water causes a cold water current flowing downwards along the sloping bottom and penetrating into the deeper regions. After a sufficient time a quasi-steady state

See http://anziamj.austms.org.au/ojs/index.php/ANZIAMJ/article/view/76 for this article, Published January 11, 2008. ISSN 1446-8735

is attained and at the end two main fluid layers are developed: a relatively stable undercurrent, and a very unstable return flow just below the water surface. Numerical results for different Grashof numbers are discussed. Understanding of the flow mechanisms pertinent to this flow is important for predicting the transport of nutrients and pollutants across the reservoir.

Contents

1 Introduction

Diurnal heating and cooling of the side arms of lakes and reservoirs with gently sloping bottoms may result in large scale convective circulations. Typically, the input of solar radiation through the surface in the daytime results in relatively warm shallow regions; conversely, night time cooling through

the surface results in relatively cool shallow regions. The resulting horizontal temperature gradients generate convective motions which influence the transport of nutrients and pollutants between the near shore and central regions of the water body, and therefore play a central role in the water quality.

Horsch and Stefan [1] investigated numerically and experimentally the convective circulation in littoral waters due to surface cooling in a triangular enclosure. Their results illustrated the development of the flow including the formation of sinking thermals and the establishment of a full cavity scale circulation. Their work was later followed by Lei and Patterson [2], who presented scaling analysis which revealed three laminar flow regimes, namely conductive, transitional and convective regimes, depending on the Rayleigh number. Their numerical simulations verified their scaling predictions. Earlier the same authors [3] studied the effect of day-time heating induced natural convection in a shallow wedge. Later, they investigated flow responses to periodic heating and cooling in a reservoir [4]. The numerical results showed a time lag in the response of the overall flow when thermal forcing was switched between heating and cooling. This was consistent with the field observations of Adams and Wells [5] and Monismith et al. [6], and the analysis of Farrow and Patterson [7, 8]. They also concluded that during both the cooling and heating phases thermal instabilities break the residual circulation and reverse the flow in deep waters.

Most of the above mentioned works (except [4]) were confined to a triangular cavity, which is a poor geometric representation of the real system. The present article extends those works with a numerical simulation of an extended system with the addition of an adjacent region of uniform water depth, which is a more realistic model, under constant surface cooling.

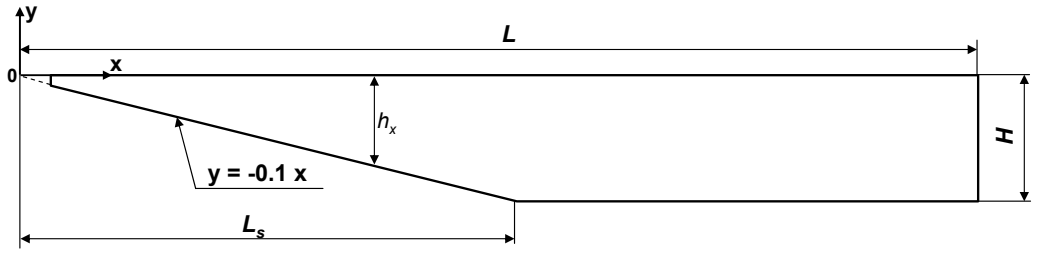

FIGURE 1: Schematic of the system considered.

2 Numerical model and procedures

Figure 1 shows the two dimensional reservoir model used in the numerical simulations. It consists of two regions: a region with a sloping bottom, and an adjacent region with an uniform water depth. The total length of the model is L with a maximum depth H. The sloping bottom region ends at $x = L_s$, and the parameter h_x denotes the local water depth. The origin of the coordinates is at the tip of the triangular region. The system is then subjected to a constant, negative heat flux at the water surface, $y = 0$. The average water temperature in the system is therefore constantly decreasing due to the heat loss through the surface.

The flow modes and temperature evolutions are governed by the usual continuity (1), Navier–Stokes (2) and energy (3) equations. They are written for an incompressible Newtonian fluid with the Boussinesq assumption:

$$\nabla \cdot \vec{u} = 0\,, \tag{1}$$

$$\frac{\mathrm{D}\vec{u}}{\mathrm{D}t} = -\frac{1}{\rho_0}\nabla p + \nu\nabla^2\vec{u} + g\beta(T - T_0)\begin{pmatrix}0\\1\end{pmatrix}, \tag{2}$$

$$\frac{\mathrm{D}T}{\mathrm{D}t} = k\nabla^2 T\,, \tag{3}$$

where $\vec{u}$ is the fluid velocity, t is the time, p is the pressure, T is the temperature, ρ_0 the density at the reference temperature T_0, k the thermal diffusivity,

g the gravitational acceleration, β is the thermal expansion coefficient and ν is the kinematic viscosity.

The boundary conditions are rigid, no-slip and adiabatic walls on the bottom and deep end and stress free and iso flux at the water surface. Thus for $y = -Ax\,,\ 0 \le x \le L_s$ and $y = -h\,,\ L_s \le x \le L\,,$

$$\vec{u} = 0\,, \quad \frac{\partial T}{\partial \vec{n}} = 0\,, \tag{4}$$

where $\vec{n}$ is normal to the bottom surface. For $y = 0$:

$$v = 0\,, \quad \frac{\partial u}{\partial y} = 0\,, \quad \frac{\partial T}{\partial y} = -\frac{H_0}{k} + \epsilon\left[\text{random}\,(0,1) - 0.5\right]\frac{H_0}{k}\,. \tag{5}$$

Here, u and v are the horizontal and vertical components of velocity respectively, random $(0,1)$ is a random number between 0 and 1 with non specific time variation and computed for every grid point at the top surface boundary, $H_0 = I_0/\left(\rho_0 C_p\right)$, I_0 is the fixed surface heat flux, and C_p is the specific heat at the reference temperature. The parameter ϵ specifies the intensity of the random perturbation to the surface boundary condition which triggers any instabilities. In these simulations $\epsilon = 2\%$. Initially, the water is stationary $(\vec{u} = 0)$, and isothermal $(T = T_0)$.

Equations (1)–(3) were numerically solved using the commercial finite volume package FLUENT 6.2 [9]. Two dimensional, unsteady, second order, time formulations were employed in all subsequent computations. Pressure-velocity coupling was obtained using the SIMPLE method [10] with spatial derivatives approximated using a second order, upwind scheme.

For easier characterization of the unsteady natural convection, four non-dimensional parameters are defined. They quantify the important properties of the fluid and the flow. These are the Prandtl number, the Grashof number, the aspect ratio and the bottom slope:

$$\text{Pr} = \frac{\nu}{k}\,, \quad \text{Gr} = \frac{g\beta H_0 h^4}{\nu^2 k}\,, \quad A = \frac{H}{L}\,, \quad A_s = \frac{H}{L_s}\,. \tag{6}$$

For all computed cases with water as a medium, the Prandtl number has a constant value of 7.07. The numerical computations were carried out for Grashof numbers $\mathrm{Gr} = 10^5$, 10^6, 10^7, and 5×10^7 to examine flow responses with different strengths of the surface cooling. The aspect ratio in all cases is fixed at $A = 0.05$ and the bottom slope at $A_s = 0.1$. The horizontal volumetric flow rate across a vertical sectional plane at a given x location is defined as

$$Q(x) = \frac{1}{2} \int_{-h_x}^{0} |u| \, dy \, . \tag{7}$$

The averaged volumetric flow rate Q_m is obtained by integrating these quantities along the horizontal direction:

$$Q_m = \frac{1}{L} \int_0^L Q(x) \, dx = \frac{1}{2L} \int_0^L \int_{-h_x}^{0} |u| \, dy \, dx \, . \tag{8}$$

In the above equations $Q(x)$ and Q_m are normalized using the scale k.

3 Results and discussion

The results of the numerical simulation are presented here. First, the averaged horizontal volumetric flow rate Q_m, which is a quantity of the greatest interests in applications dealing with transport of nutrients and pollutants in coastal waters, is presented for several Grashof numbers. Second, the flow development at $\mathrm{Gr} = 10^7$ is presented in detail. Finally, the quasi-steady flows for three different Grashof numbers are compared with each other.

In all of the simulations, the reference temperature is set to $T_0 = 20°\mathrm{C}$, and the dimensions of the model are fixed at $L = 2\,\mathrm{m}$, $L_s = 1\,\mathrm{m}$ and $H = 0.1\,\mathrm{m}$. These correspond to the values used in an experimental program, which will be reported separately.

Before the computations were carried out, a grid dependency test was conducted. The averaged volumetric flow rate Q_m was compared for this

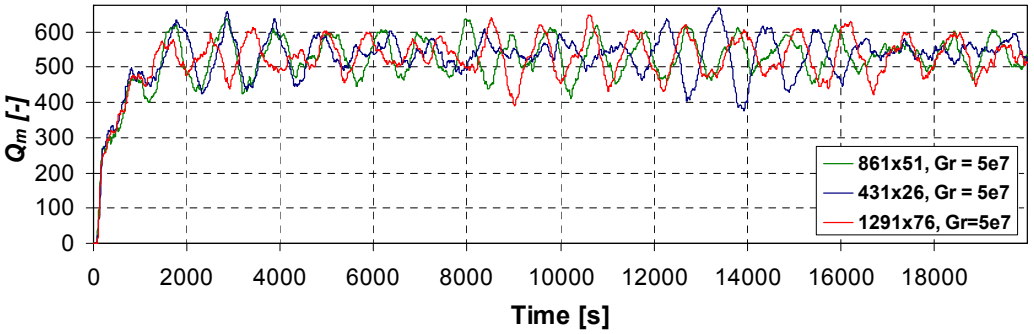

FIGURE 2: Transient responses of the averaged volumetric flow rates at $\mathrm{Gr} = 5 \times 10^7$, $\mathrm{Pr} = 7.07$ and for three different mesh sizes: 861×51, 431×26 and 1291×76.

purpose. Three non-uniform meshes (431×26, 861×51 and 1291×76) were constructed to examine the dependence of the numerical solutions on the grid resolution for $\mathrm{Gr} = 5 \times 10^7$ and $\mathrm{Pr} = 7.07$. Figure 2 shows the transient response of the averaged volumetric flow rate obtained with the three different meshes. Observe that the overall flow development is comprised of three distinct stages, that is, an early stage with the volumetric flow rate increasing steadily, a transitional stage with the volumetric flow rate continuing to increase but subject to fluctuations, and a quasi-steady stage with the volumetric flow rate fluctuating about a constant mean value. In the early stage of the flow development, the three solutions with different meshes follow nicely with each other. However, they start to diverge during the transitional stage. Despite the fluctuations of the solutions about an approximately same mean value at the quasi-steady stage, the occurrence of peaks and troughs in the three solutions is arbitrary. The divergence of the numerical solutions with different meshes at the transitional and quasi-steady stages is caused by the flow instabilities, which is discussed later in this article. We show later that the flow instabilities originate from the cooling layer underneath the water surface and take the form of plunging thermals, which is arbitrary in nature. This type of flow instabilities is extremely sensitive to the mesh

TABLE 1: Mesh dependency test for $\mathrm{Gr} = 5 \times 10^7$.

Mesh size	Q_m	Max. variation
431×26	537.64	
861×51	535.28	1.78%
1291×76	528.08	

resolution. Since this study is concerned with understanding the overall flow development rather than resolving the details of the flow instability, the time averaged volumetric flow rate at the quasi-steady state is considered for comparison purpose. The calculated, time averaged, volumetric flow rates with the three meshes are listed in Table 1. We understand that this quantity is very sensitive to the time period over which the volumetric flow rate is averaged. This factor may have directly contributed to the relatively large variation of the solution with the finest mesh from the other two solutions. Nevertheless, the variation of the calculated, time averaged, volumetric flow rate between the two fine meshes is only less than 1.4%. In consideration of the significant computing resources required for the finest mesh, the medium mesh (861×51) is adopted for all subsequent computations. Similarly, a time step test was carried out for the largest Grashof number case. Six different time steps ($t = 0.05, 0.1, 0.2, 0.5, 1.0, 2\,\mathrm{s}$) were tested. Based on this test, a time step of 0.2 s was adopted for all subsequent calculations.

3.1 Horizontal exchange flow rates

Figure 3 shows the time histories of the integrated volumetric flow rates at $\mathrm{Pr} = 7.07$ and $\mathrm{Gr} = 10^5, 10^6, 10^7$ and 5×10^7 respectively. We see that the intensity of the flow response increases with the Grashof number (stronger cooling results in faster flow exchange and quicker initialization of the flow). For lower Grashof numbers the flow responses appear to be smooth; however, at larger Grashof numbers the integral volumetric flow rates show clear oscillatory behaviour (here strongest at $Gr = 5 \times 10^7$). The presence of this

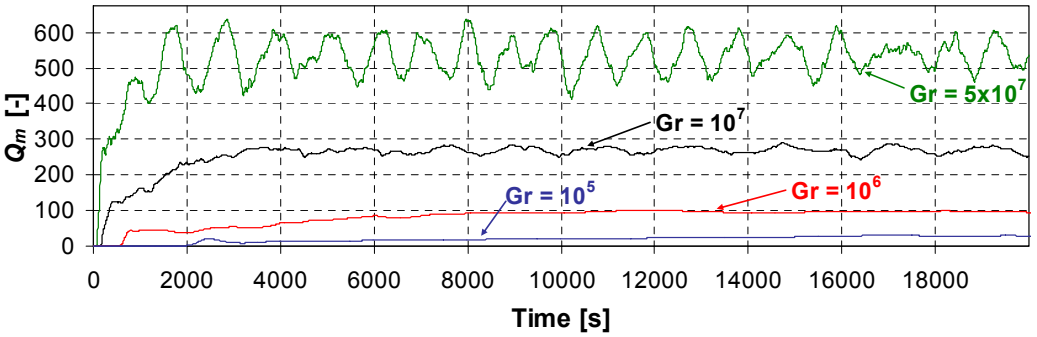

FIGURE 3: Transient responses of the averaged volumetric flow rates for different Grashof numbers $\mathrm{Gr} = 10^5, 10^6, 10^7$ and 5×10^7.

oscillatory behaviour is discussed in the following section. We see from these plots that there are three distinct stages of the flow development: an initial stage, a transitional stage and a quasi steady stage. The first stage describes the creation of the initial boundary layer (conductive effect). In the second stage onset of initial instabilities occurs and a relatively stable undercurrent and unstable thermals develop in the domain. The last stage represents a fully developed convective circulation.

3.2 Flow structures

3.2.1 Initial stage flow at $\mathrm{Gr} = 10^7$

Initially, the heat loss through the water surface creates a horizontal conductive boundary layer just below the water surface as seen in Figure 4. In this, and all subsequent figures, blue colour always represents relatively cold regions and red colour relatively warmer water regions. As the article considers general characteristics of the fluid flow in reservoir, the isotherms are always scaled in a way to present clearly the flow evolution depending on the

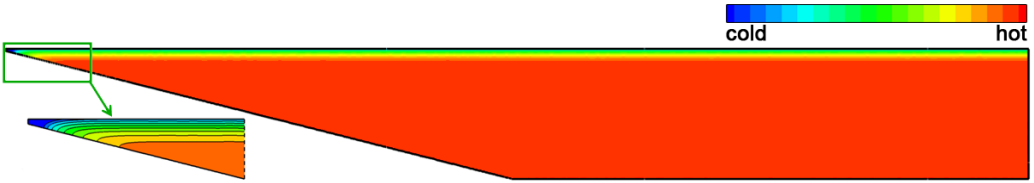

FIGURE 4: Isothermal contours at the initial stage of the flow development (conductive effect) at $\mathrm{Gr} = 10^7$, $\mathrm{Pr} = 7.07$ and $t = 120\,\mathrm{s}$.

Grashof number. In the shallow region the isotherms are deformed in order to satisfy the no-flux boundary condition on the sloping bottom and they curl over to become perpendicular to the slope. This generates a temperature gradient along the sloping bottom which is responsible for a later convective flow of relatively colder water down the slope into the deeper regions. Further, the volumetric cooling rate decreases with increasing water depth since the surface heat flux is constant. This further reinforces the convective circulation.

3.2.2 Transitional stage flow at $\mathrm{Gr} = 10^7$

Shortly after the initialization of the flow, sinking cold water plumes originating from the conductive surface layer are observed in Figure 5a. These are due to the cooling of the water body from above which makes the fluid at the surface more dense. When the cooling is strong enough the thermals start to penetrate the local water depth. The plunging thermals are responsible for the initial mixing of the fluid and their initial wavenumber depends on the local rate of cooling. Those thermals located closer to the tip reach the slopping bottom sooner, and, through the enhanced mixing, accelerate the development of the convective circulation in the system.

With increasing time the plumes described above tend to merge together, creating larger structures. They penetrate the local water depth carrying

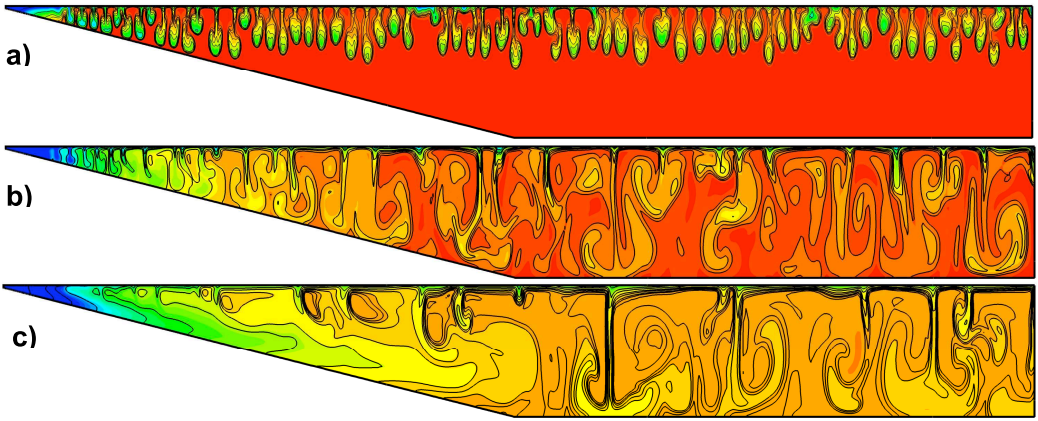

FIGURE 5: Isothermal contours at the transitional stage at $\mathrm{Gr} = 10^7$, $\mathrm{Pr} = 7.07$ and a) $t = 220\,\mathrm{s}$; b) $t = 400\,\mathrm{s}$; c) $t = 1200\,\mathrm{s}$;.

relatively colder fluid toward the bottom, where they are prone to overturning, and mixing with ambient fluid as seen in Figure 5b. During this process, plunging thermals continuously change their forms. They often appear straight, but sometimes are curved with no apparent regularity and pattern of movement. Thermals sinking in the shallow region cool that area faster and a cold undercurrent is created gradually on the slope. That undercurrent slowly proceeds towards the deeper region, being constantly fed by a return flow of cold water along the surface. As seen in Figure 5c the undercurrent reaches the end of the sloping region. At this moment it is possible to observe three main regions of the flow: the undercurrent on the sloping bottom, a surface return flow which is moving under the water surface toward the shallow end, and the deep region with large sinking plumes. The thermals above the slope are becoming weaker and deformed by the undercurrent.

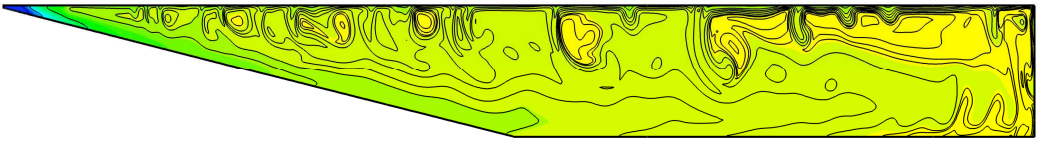

FIGURE 6: Isothermal contours at $\mathrm{Gr} = 10^7$, $\mathrm{Pr} = 7.07$ and $t = 8000\,\mathrm{s}$.

3.2.3 Quasi-steady stage flow at $\mathbf{Gr} = 10^7$

After some time, the undercurrent reaches the vertical adiabatic wall and a quasi-steady state is attained. The average temperature of the entire domain is still constantly decreasing; however, the averaged horizontal flow rate is almost constant. Figure 6 shows isotherms at the quasi-steady state ($t = 8000\mathrm{s}$). The relatively stable undercurrent is easily observed along the bottom. The return flow, unlike the undercurrent, is very unstable as the surface is being continuously cooled. Sinking plumes burst periodically from the return flow below the water surface.

3.2.4 Dependence on the Grashof number

Figure 7 shows isothermal contours in the quasi-steady stage for three different cooling rates: $\mathrm{Gr} = 10^5$, 10^6 and 5×10^7. Although the times selected for presenting the data are different, the flows are at comparable stages of development. Of particular interest is a comparison of the undercurrent and the surface return flow in each case. When the cooling rate is low ($\mathrm{Gr} = 10^5$, 10^6), the undercurrent layer is thicker and more stable. The return flow is constantly disturbed by sinking plumes, but the influence of the plumes on the undercurrent is relatively weak. However, in Figure 7c ($\mathrm{Gr} = 5 \times 10^7$) the undercurrent is noticeably disturbed by the thermals coming from the above and the undercurrent separates from the bottom in a complex interaction with the plumes. However, the flow maintains the general characteristic of having two convective layers. The disturbances in the form of sinking

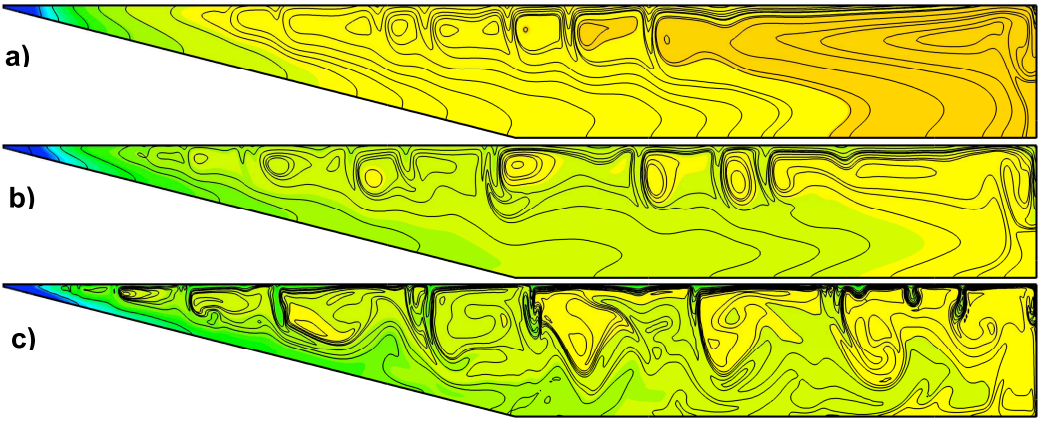

FIGURE 7: Isothermal contours in quasi-steady state at Pr = 7.07 and a) Gr = 10^5, t = 83880 s; b) Gr = 10^6, t = 20000 s and c) Gr = 5×10^7, t = 4100 s.

plumes create strong oscillatory behaviour of the integrated flow rates, as seen in Figure 3.

4 Summary

This article describes a numerical investigation of the flow in shallow waters with a gently sloping bottom subject to constant cooling at the water surface. An understanding of the mechanisms of such exchange flows is central to modelling the transport of nutrients and pollutants in lakes and reservoirs. The mechanisms for the creation of the horizontal thermal boundary layer and the formation of the sinking plumes are described. The detailed flow development is presented for Gr = 10^7. We have shown that two main distinct layers developing in the resulting convective circulation; an undercurrent along the bottom and an unstable return flow under the water surface. The stability of the return flow strongly depends on the cooling rate.

The unsteady flow structures obtained in the present numerical simulations were also observed in our recent experimental investigation [11]. The experimental results clearly showed different stages of the flow development similar to those presented above. Both experimental and numerical results indicate that the convective motions in reservoirs induced by night-time cooling have a significant impact on water quality and transport of nutrients and pollutants.

Acknowledgment This research is supported by the Australian Research Council.

References

[1] G. M. Horsch, H. G. Stefan, Convective circulation in littoral water due to surface cooling, *Limnol. Oceanogr.*, **33**, 1998, 1068–1083. C854

[2] C. Lei, J. C. Patterson, Unsteady natural convection in a triangular enclosure induced by surface cooling, *Int. J. Heat and Fluid Flow*, **26**, 2005, 307–321. C854

[3] C. Lei, J. C. Patterson, A direct three-dimensional simulation of radiation-induced natural convection in a shallow wedge, *Int. J. Heat and Mass Transfer*, **46**, 2003, 1183–1197. doi:10.1016/S0017-9310(02)00401-5 C854

[4] C. Lei, J. C. Patterson, Natural convection induced by diurnal heating and cooling in a reservoir with slowly varying topography, *JSME International Journal, Series B: Fluids and Thermal Engineering*, **49**(3), 2006, 605–615. doi:10.1299/jsmeb.49.605 C854

[5] E. E. Adams, S. A. Wells, Field measurements on side arms of Lake Anna Va, *J.Hydraulic Eng.*, **110**, 1984, 773–793. C854

[6] S. G. Monismith, J. Imberger, M. L. Morison, Convective motions in the sidearm of a small reservoir, *Limnol. Oceanogr.*, **35**(8), 1990, 1676–1702. C854

[7] D. E. Farrow, J. C. Patterson, On the response of a reservoir sidearm to diurnal heating and cooling, *J. Fluid Mech.*, **246**, 1993, 143–161. doi:10.1017/S0022112093000072 C854

[8] D. Farrow, Periodically forced natural convection over slowly varying topography, *J. Fluid Mech.*, **508**, 2004, 1–21. doi:10.1017/S002211200400847X C854

[9] FLUENT 6.2 *User's guide*, Fluent Inc., Lebanon, 2005. C856

[10] H. K. Versteeg, W. Malalasekera, *An introduction to computational fluid dynamics: the Finite Volume method*, Longman Scientific and Technical, 1995. C856

[11] T. P. Bednarz, C. Lei, J. C. Patterson, An experimental study of unsteady natural convection in a reservoir model cooled from the water surface, *Experimental Thermal and Fluid Science*, **32**, 2007, 844–856. doi:10.1016/j.expthermflusci.2007.10.007 C865

Author addresses

1. **Tomasz P. Bednarz**, James Cook University, School of Engineering, Townsville, Queensland 4811, Australia.
mailto:tomasz.bednarz@jcu.edu.au

2. **Chengwang Lei**, James Cook University, School of Engineering, Townsville, Queensland 4811, Australia.
mailto:chengwang.lei@jcu.edu.au

3. **John C. Patterson**, James Cook University, School of Engineering, Townsville, Queensland 4811, Australia.
mailto:john.patterson@jcu.edu.au